
















# An Algorithm for the Efficient Management of the Power Converters Connected to the DC Bus of a Hybrid Microgrid Operating in Grid-connection Mode

Robert Salas-Puente, Silvia Marzal, Raúl González-Medina, Emilio Figueres, and Gabriel Garcerá

## QUERY SHEET

This page lists questions we have about your paper. The numbers displayed at left can be found in the text of the paper for reference. In addition, please review your paper as a whole for correctness.

- Q1. Au: Please check running head is ok ? 
- Q2. Au: Please note that the Funding sections have been created from information supplied during the peer review process, not from your manuscript. Please correct if this is inaccurate.       
- Q3. Au: Please provide issue number and month of publication for reference [1], [2], [3], [4], [5], [6], [7], [8], [11], [12], [13], [14], [16].       


## TABLE OF CONTENTS LISTING

The table of contents for the journal will list your paper exactly as it appears below:

**An Algorithm for the Efficient Management of the Power Converters Connected to the DC Bus of a Hybrid Microgrid Operating in Grid-connection Mode**  
*ROBERT SALAS-PUENTE, SILVIA MARZAL, RAÚL GONZÁLEZ-MEDINA, EMILIO FIGUERES, AND GABRIEL GARCERÁ*



# An Algorithm for the Efficient Management of the Power Converters Connected to the DC Bus of a Hybrid Microgrid Operating in Grid-connection Mode

Robert Salas-Puente , Silvia Marzal, Raúl González-Medina, Emilio Figueres, and Gabriel Garcerá

Grupo de Sistemas Electrónicos Industriales del Departamento de Ingeniería Electrónica, Universitat Politècnica de València, Camino de Vera s/n, Valencia, España

## CONTENTS

- 1. Introduction
- 2. Description of the Hybrid Microgrid Under Study
- 3. Management and Control of the HY MG
- 5 4. Simulation and Experimental Results and Discussion
- 5. Conclusions
- Funding
- References

**Abstract**—In this paper a centralized control strategy for the efficient power management of the power converters conforming a hybrid distributed generation microgrid is explained. The microgrid is based on a DC and an AC bus. The study is focused on the converters connected to the DC bus. The proposed power management algorithm is implemented in a microgrid central processor. This algorithm is based on assigning several operation functions to each of the generators, loads and energy storage systems in the microgrid. A communication system is used to assign the operation functions to each of the microgrid elements. The power flows between the DC and AC buses are studied in several operation scenarios, in which the proposed control can be verified.

Experimental and simulation results demonstrate that the algorithm allows to control the power dispatch inside the microgrid properly, by performing the following tasks: (1) the communications among power converters, the grid operator and intelligent loads, (2) the connection and disconnection of loads, (3) the control of the power exchange between the distributed generators and the energy storage system, (4) the compliance of the power dispatch limit set by the grid operator, (5) the synchronization with the grid and (6) the control of the voltage at the DC bus.

## 1. INTRODUCTION

Most countries are dependent on fossil fuels and nuclear energy for electric power generation. However, due to the increasing energy demand and the proliferation of new forms of energy generations which are cheaper and environment-friendly, many distributed generation (DG) systems have been integrated in the power grid [1]. Some DGs consist in Renewable Energy Sources (RES), such as: Photovoltaic (PV), wind, biomass, geothermal [2], [3]. The DGs are the basis of Microgrids (MGs), which can operate as a single power system that provides a safe and reliable operation

Keywords: power management, microgrids, communications, energy storage systems, photovoltaics, power converters

Received 31 October 2016; accepted 24 March 2018

Address correspondence to Grupo de Sistemas Electrónicos Industriales del Departamento de Ingeniería Electrónica, Universitat Politècnica de València, Camino de Vera s/n, 46022, Valencia, España. E-mail: rosapuel@posgrado.upv.es

Color versions of one or more of the figures in the article can be found online at [www.tandfonline.com/uemp](http://www.tandfonline.com/uemp).

at certain voltage and load levels [4]. An MG may work in island mode or in grid-connected mode, so that it can connect to DGs placed at various locations and inject their energy to the grid if needed [5]. There are three basic MG topologies, which can be classified according to the nature of their voltage: DC microgrid (DC MG) [6], [7], AC microgrid (AC MG) [8], and hybrid microgrid (HY MG), which is an MG with AC and DC buses. HY MGs are currently of great interest to researchers and are considered the distribution and transmission systems of the future, because they enable the coexistence of both AC MGs and DC MGs [9]–[11]. The main drawback of HY MGs is the large amount of complex power electronics interfaces required, that may complicate the control, management, communication and power dispatch among devices. Besides, the protection strategy of HY MGs is more complex than that of traditional MG [12], [13].

Early proposals for the control of an HY MG were shown in [9]–[11]. In [14] a decentralized control of a MG is proposed using an interlinking converter (ILC) in order to coordinate the power flows among the power converters connected to the AC and DC buses. Droop methods [15] were used to share the power delivered by the converters under operation. Droop was applied in [14] to the power converters connected both to the DC and to the AC bus. That control concept was extended in [16] and [17] to implement the power interchange among the subgrids conforming a HY MG. Several studies about power management in HY MGs using droop strategies for the power dispatch have been recently presented [18]. In [19] the droop concept is extended in combination with a cost function defined for the power dispatch.

In that work a different approach to the power dispatch inside the HY MG is used, because a centralized control decides the status of the DGs, the loads and the energy storage system (ESS) in the MG by applying a set of predefined operation functions to each of the elements under operation. The approach of this paper is based on secure communications between the microgrid elements and a microgrid central processor (MGCP).

The main contributions of this manuscript are:

- (1) The comprehensive design of a practical power management algorithm which is programmed inside an MGCP.
- (2) The definition of a set of twelve operation functions for each of the microgrid elements: generators, loads and energy storage systems. Those functions are chosen by the MGCP in real time and broadcasted by the MGCP to the MG elements in order to set their status.
- (3) The definition of hysteresis levels for the comparison with the power thresholds which determine a change of the functions to be applied to the MG elements.

- (4) Compliance of the power dispatch limits established by the grid operator regarding the power flow between the HY MG and the public grid.
- (5) The evaluation on an experimental platform of the proposed algorithm in several MG scenarios.

The MGCP sets the operation mode of each device connected to the HY MG by means of an RS485 serial communications system implemented on the MODBUS [20] protocol. MODBUS has a suitable performance in the MG environment [21], incorporating a cyclic redundancy code (CRC) to check the message integrity. A floating point TMS320F28335 DSP inside each of the power converters under operation has been used to implement the corresponding inner controllers. The power management algorithm has been implemented in an MGCP based on a TMS320F28335 DSP running at 150 MHz. This paper consists of 5 sections. After the introduction of section 1, in section 2 a general description of the HY MG under study is provided. In section 3 several concepts of the power management algorithm are explained, like its structure, system parameters, priority variables, limitations and the operation functions applied by the MGCP. In section 4 simulation and experimental results at different scenarios of the MG are presented. In section 5 the conclusions of the study are presented.

## 2. DESCRIPTION OF THE HYBRID MICROGRID UNDER STUDY

The proposed HY MG is depicted in Figure 1. The parameters of the communication system inside the MG are shown in Table 1. The nomenclature used in this paper is listed in Table 2. The HY MG under study is based on a single DC bus and a single AC bus, connected to the PCC of the public grid by means of a static switch. The connection of the DC and AC buses is performed by an ILC, allowing a bidirectional power flow. In grid connected mode the ILC may work as a current source that injects power to the grid synchronously with the AC bus voltage. The MGCP sets the operation functions of each of the power converters, loads, and the ESS as a function of the MG scenarios. These scenarios depend on internal and external changes that affect the dispatchable power, such as changes of the solar irradiation, of the load, of the power limit established by the public grid operator and of the ESS batteries state of charge (SOC).

The MGCP achieves a suitable power dispatch by broadcasting several control actions to the microgrid devices: (a) connection/disconnection of the loads as a function of the generated power and the available energy stored in the batteries, (b) distribution of the available power between the

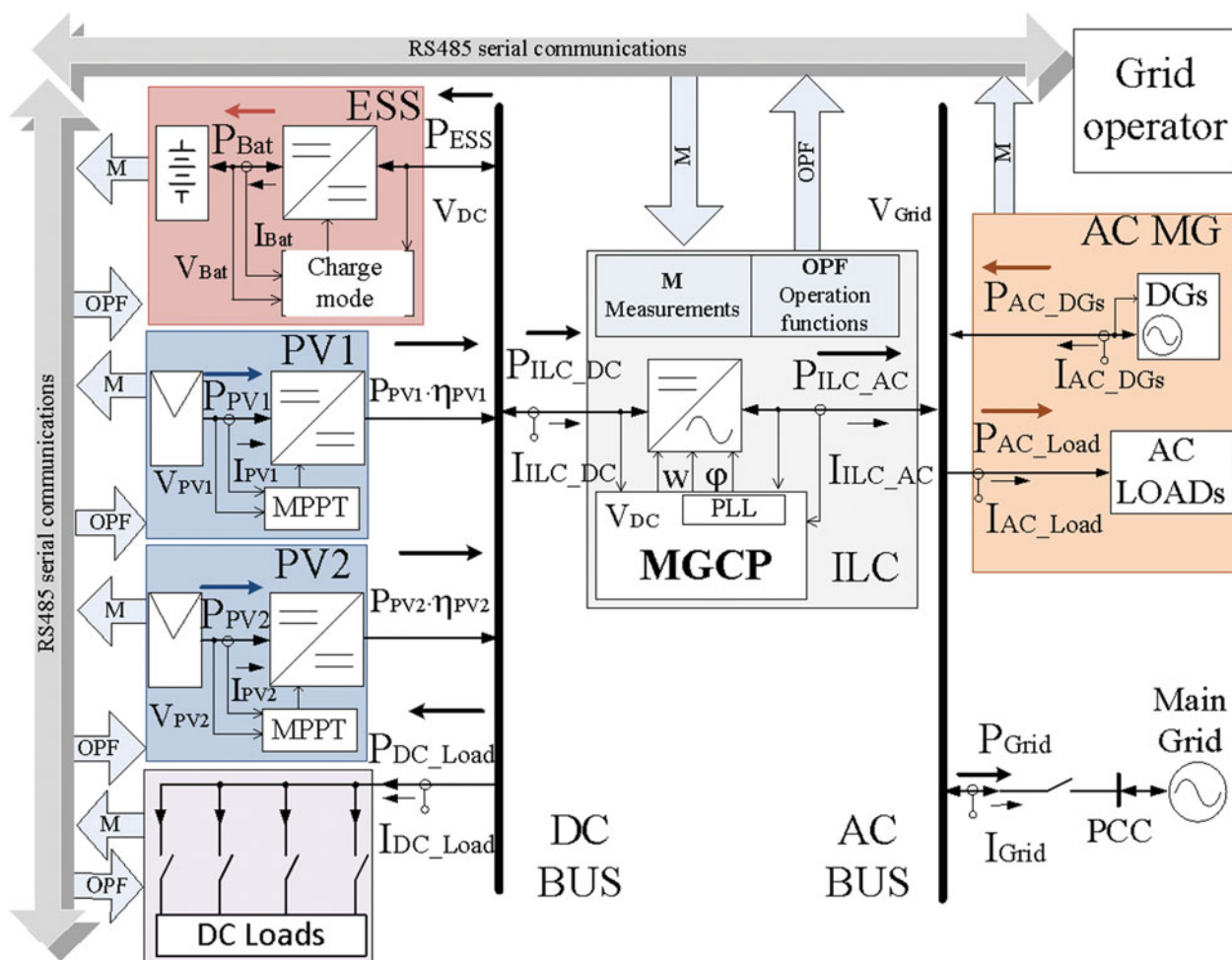


FIGURE 1. Conceptual scheme of the hybrid microgrid under study.

Communication parameters between the devices of the HY MG and the MGCP

	DC MG				AC MG	
	ESS	ILC	PV	Load	DGs	Load
<b>Operations functions</b>	$V_{DC\_ref}$	$\varphi$	$P_{PV\_Lim}$	$SW_{1\_Load\_DC}$		
	$I_{Dis\_ref}$	$\omega$		$SW_{2\_Load\_DC}$		
	$I_{Ch\_ref}$	$V_{DC\_ref}$		$SW_{3\_Load\_DC}$		
	$VC$			$SW_{4\_Load\_DC}$		
<b>Measurements</b>	$Z_3$					
	$I_{Bat}$	$I_{ILC\_AC}$	$I_{PV1}$	$I_{DC\_Load}$	$I_{AC\_DGs}$	$I_{AC\_Load}$
	$V_{DC}$	$V_{DC}$	$V_{PV1}$		$V_{Grid}$	$V_{Grid}$
	$V_{Bat}$	$V_{Grid}$	$I_{PV2}$			
	$SOC$		$V_{PV2}$			

Communication parameters between the MGCP and the grid operator

High-level control

EDL,  $\hat{P}_{Grid-to-MG}$ ,  $\hat{P}_{MG-to-Grid}$

TABLE 1. Communication parameters of the system.

## 4 Electric Power Components and Systems, Vol. 0 (2018), No. 0

$P_{PV1}, P_{PV2}$	Power supplied by the PV arrays 1 and 2
$P_{PV}$	PV power generated by the DC MG
$P_{DCLoad}$	Overall power consumed by the DC loads
$P_{Grid}$	Power injected from the HY MG to the grid
$P_{ILC\_AC}$	Power injected from the DC bus to the AC bus by the ILC, measured at the AC side of the ILC
$P_{ILC\_DC}$	Power injected from the DC bus to the AC bus by the ILC, measured at the DC side of the ILC
$P_{ESS}$	Battery bank charge power seen from the DC bus
$P_{Bat}$	Battery bank charge power
$P_{ACLoad}$	Overall power consumed by the AC loads
$P_{AC\_DGs}$	Power supplied by the AC DGs
$\eta_{EES}$	Efficiency of the ESS
$\eta_{PV1}, \eta_{PV2}$	Efficiency of the PV DC–DC converters 1 and 2
$\eta_{ILC}$	Efficiency of the ILC
$I_{Grid}$	RMS Current injected from the HY MG to the grid
$V_{Grid}$	RMS value of the grid voltage
$\omega$	Grid angular frequency
$\varphi$	Grid phase
$I_{ACLoad}$	Overall RMS current consumed by the AC loads
$I_{DCLoad}$	Overall current consumed by the DC loads
$V_{DC}$	DC bus voltage
$I_{ILC\_AC}$	RMS current injected from the ILC to the AC bus
$SOC$	State of charge of the battery bank
$I_{Bat}$	Battery bank charge current
$V_{Bat}$	Battery bank voltage
$I_{Ch\_ref}$	Reference of the battery charge current
$I_{Dis\_ref}$	Reference of the battery discharge current
$I_{PV1}, I_{PV2}$	Current supplied by the PV arrays 1 and 2
$P_{PV\_Lim}$	Required PV power limit
$I_{DCLoad}$	Overall current consumed by the DC loads
$S_{W1,2,3,4DC\_Load}$	DC load switches (load 1 to 4)
$EDL$	Energy dispatch limit
$\hat{P}_{Grid-to-MG}$	Maximum power drawn from the grid to the HY MG
$\hat{P}_{MG-to-Grid}$	Maximum power injected to the grid from the HY MG
$\hat{P}_{ILC\_AC Grid-to-MG}$	Maximum power drawn from the AC bus to the DC bus measured at the AC side of the ILC
$\hat{P}_{ILC\_AC MG-to-Grid}$	Maximum power injected from the DC bus to the AC bus measured at the AC side of the ILC
$P_{ILC\_AC-Rated}$	Rated power of the ILC measured at its AC side
$P_{ILC\_DC-Rated}$	Rated power of the ILC measured at its DC side
$\hat{P}_{DC\_Load}$	Maximum power consumed by the DC loads
$P_{Available\_DCMG}$	Power available at the DC bus of the HY MG
$DC_{Load\_hyst}$	DC load hysteresis
$PESS_{C10}$	Power drawn by the ESS from the DC bus at a battery charge current equal to C10

TABLE 2. Nomenclature.

140 critical loads and the ESS, (c) definition of hysteresis lev-  
 145 els in the comparison with power thresholds which define a  
 change of the operation mode of the MG elements, so that  
 a stable DC bus voltage is obtained, and (d) compliance of  
 the power limits established by the grid operator regarding  
 power import/export from/to the public grid. Note that the grid  
 operator can establish different power exchange limits in any  
 moment by means of serial communications. Obviously, the  
 power generated by the energy sources connected to the DC  
 bus must be limited by the MGCP to prevent an excessive

power injection to the public grid beyond the limit set by the 150  
 grid operator.

The MGCP defines the internal functionality depending on  
 the possible scenarios of the HY MG. The communications  
 allow controlling the PV DGs, the ESS and the load connec-  
 155 tion/disconnection. In Figure 1a 10 kW ILC, which connects  
 the AC bus and the DC bus, can be observed. The AC bus is  
 single phase and works in grid-connected mode with a grid  
 voltage:  $V_{Grid} = 230 V_{rms}$  and  $F_{Grid} = 50 Hz \pm 1 Hz$ . In the  
 HY MG under study two additional elements are connected to



160 the AC bus: a 5 kW AC DG, and a 4 kW AC load. The nominal  
DC bus voltage is  $V_{DC} = 420$  V, being regulated by the ILC.  
Three elements are connected to the DC bus: a 3 kW bidi-  
rectional DC–DC converter connected to a battery bank and  
two 5 kW DC–DC converters connected each one to one PV  
165 array. The voltage at the battery bank ( $V_{Bat}$ ) ranges from 192 V  
to 252 V, whereas the voltages at the PV arrays ( $V_{PV1}$  and  
 $V_{PV2}$ ) vary from 306 V to 378 V. Additionally four ‘shed-able’  
2 kW DC loads are connected to the DC bus. The loads can  
be connected or disconnected to/from the DC-bus by means  
170 of individual switches controlled by the MGCP ( $Sw1_{LoadDC}$  to  
 $Sw4_{LoadDC}$ ).

### 3. MANAGEMENT AND CONTROL OF THE HY MG

#### 3.1. Parameters of the MGCP

175 In this section several concepts and parameters of the MGCP  
are explained, in order to define the features and control func-  
tionalities of the HY MG for the efficient application of the  
proposed algorithm.

3.1.1. *High-Level Control Limits.* The main grid operator  
establishes a tertiary high-level control strategy which con-  
180 trols the power flow between the HY MG and the grid. That  
power flow imposes a limit of the power injected from the HY  
MG to the grid or vice versa. The limits from the high-level  
control are:

3.1.1.1. *Energy Dispatch Limit (EDL).* EDL is a digital  
185 flag that tells the MGCP if there exists an energy dispatch  
limit in the MG. EDL allows the MGCP to set a suitable con-  
trol strategy by taking into account the values of the maximum  
power extracted/injected from/to the grid to/from the HY MG.  
When  $EDL = Off$  there is no energy dispatch limit and the  
190 MGCP can inject or extract unlimited power to/from the grid.  
In the opposite case ( $EDL = On$ ) the MGCP establishes a set  
of power management criteria which depend on the load con-  
nected to the AC or DC buses, on the power available in the  
MG and on the SOC of the batteries.

195 3.1.1.2. *Maximum Power Extracted from the Grid*  
( $\hat{P}_{Grid-to-MG}$ ). The power flow scenarios between the  
grid and the HY MG are shown in Figure 2. Two general  
cases are possible:  $P_{Grid} < 0$  and  $P_{Grid} > 0$ , being the power  
flow from the grid to the microgrid or vice versa. Parameter  
200  $\hat{P}_{Grid-to-MG}$  is established by the grid operator, standing for  
the maximum power that can be extracted from the main grid  
to the HY MG,  $|P_{Grid}| \leq \hat{P}_{Grid-to-MG}$ .

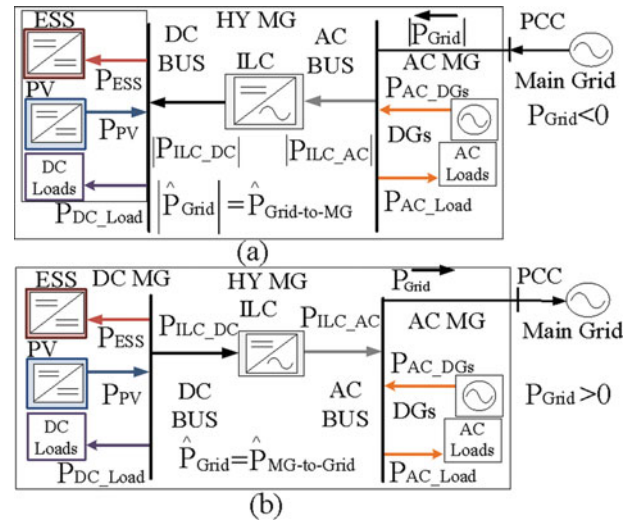


FIGURE 2. Power flow scenarios between the grid and the HY MG: (a)  $P_{Grid} < 0$ , power flow from the Grid to HY MG and (b)  $P_{Grid} > 0$ , power flow from the HY MG to Grid.

#### 3.1.1.3. Maximum Power Injected to the Grid ( $\hat{P}_{MG-to-Grid}$ ).

Parameter  $\hat{P}_{MG-to-Grid}$  stands for the maximum power that  
205 can be injected from the HY MG to the main grid. This param-  
eter is established by the grid operator, imposing condition  
 $P_{Grid} \leq \hat{P}_{MG-to-Grid}$ .

3.1.2. *Parameters of the MGCP.* The MGCP establishes  
some parameters for the secondary control strategy, which is  
210 responsible for the power flow between the AC bus and the  
DC bus of the HY MG. The MGCP must limit the power gen-  
erated by the RESs, if the available power is higher than that  
necessary at the MG buses. The secondary control parameters  
are described in the following.

3.1.2.1. *Maximum Power Extracted from the AC Bus*  
215 *to the DC Bus Measured at the AC Side of the ILC*  
( $\hat{P}_{ILC\_AC|Grid-to-MG}$ ). The power flow from the grid to the HY  
MG is depicted in Figure 2(a), in that situation the absolute  
value of  $P_{ILC\_AC}$  can be calculated by (1), where  $P_{Grid} < 0$  and  
 $P_{ILC\_AC} < 0$ . Parameter  $\hat{P}_{ILC\_AC|Grid-to-MG}$  stands for the maxi-  
220 mum power which can be extracted from the AC bus to the DC  
bus, measured at the AC side of the ILC, being given by (2).  
As the value of  $\hat{P}_{Grid-to-MG}$  is set by the MGCP, the value of  
 $\hat{P}_{ILC\_AC|Grid-to-MG}$  also depends on the MGCP. The maximum  
absolute value of  $P_{ILC\_AC}$  must meet condition (3) at any time,  
225 taking into account the rated power of the ILC. In this study:  
 $P_{ILC\_rated} = 10$  kW.

$$|P_{ILC\_AC}| = P_{AC\_DGs} + |P_{Grid}| - P_{AC\_Load} \quad (1)$$

$$\hat{P}_{ILC_{AC}|Grid-to-MG} = P_{ACDGs} + \hat{P}_{Grid-to-MG} - P_{ACLoad} \quad (2)$$

$$|P_{ILC_{AC}}| \leq MIN(P_{ILC_{AC}-Rated}, \hat{P}_{ILC_{AC}|Grid-to-MG}) \quad (3)$$

3.1.2.2. Maximum Power Injected from the DC Bus to the AC Bus Measured at the AC Side of the ILC ( $\hat{P}_{ILC_{AC}|MG-to-Grid}$ ). The power flow from the HY MG to the grid is depicted in Figure 2(b), in that situation the value of  $P_{ILC_{AC}}$  can be calculated by (4), being  $P_{Grid} > 0$  and  $P_{ILC_{AC}} > 0$ . Parameter  $\hat{P}_{ILC_{AC}|MG-to-Grid}$  stands for the maximum power which can be injected from the DC bus to the AC bus, measured at the AC side of the ILC, see (5). The maximum power injected from the DC bus to the AC bus by the ILC must meet condition in (6).

$$P_{ILC_{AC}} = P_{Grid} + P_{ACLoad} - P_{ACDGs} \quad (4)$$

$$\hat{P}_{ILC_{AC}|MG-to-Grid} = \hat{P}_{MG-to-Grid} + P_{ACLoad} - P_{ACDGs} \quad (5)$$

$$\hat{P}_{ILC_{AC}} \leq MIN(P_{ILC_{AC}-Rated}, \hat{P}_{ILC_{AC}|MG-to-Grid}) \quad (6)$$

3.1.2.3. PV Power Generated by the DC MG (PPV). Parameter  $P_{PV}$  is the overall PV power generated by the DC MG. The powers generated by the PV DGs connected to the DC bus are measured individually. The total power generated by two PV DC-DC converters connected to the DC bus is shown by (7).

$$P_{PV} = P_{PV1} \cdot \eta_{PV1} + P_{PV2} \cdot \eta_{PV2} \quad (7)$$

3.1.2.4. Power Consumed by the Loads Connected to the DC and AC Buses. The powers consumed by the loads connected to the DC bus is  $P_{DCLoad} = I_{DCLoad} \cdot V_{DC}$  and to the AC bus is  $P_{ACLoad} = I_{ACLoad_{rms}} \cdot V_{Grid_{rms}}$ .

3.1.2.5. Maximum Power Consumed by the Loads Connected to the DC bus ( $\hat{P}_{DCLoad}$ ). Parameter ( $\hat{P}_{DCLoad}$ ) stands for the maximum overall power which the DC loads is allowed to consume. The load shedding at the DC bus, performed by the MGCP, depends on this parameter.  $\hat{P}_{DCLoad} \leq P_{ILC_{DC}-Rated}$  establishes an upper limit for that maximum power as a function of the ILC power rating.

3.1.2.6. PV Power Limit ( $P_{PV\_Lim}$ ). Parameter  $P_{PV\_Lim}$  is the maximum power that should be extracted from the PV sources at any time, so that it can be consumed by the DC loads and by the batteries ( $P_{ESS} > 0$ ) and/or it injected to the grid.  $P_{PV\_Lim}$  is represented by (8), where  $P_{ESS} = (V_{Bat} \cdot I_{Bat}) / \eta_{ESS}$ .

$$P_{PV\_Lim} = \hat{P}_{ILC_{AC}|MG-to-Grid} + P_{DCLoad} + P_{ESS} \quad (8)$$

3.1.2.7. PV Generation Power Available in the DC MG ( $P_{Available\_DC\_MG}$ ). Parameter  $P_{Available\_DC\_MG}$  is the extra

power available from the PV DGs making up the DC MG after feeding the load connected in the DC bus. The available PV generation power is defined in (9).

$$P_{Available_{DC\_MG}} = P_{PV} - P_{DCLoad} \quad (9)$$

3.1.2.8. DC Load Switch. The DC load switch flag takes two possible states,  $SW_{LoadDC} = ON$  and  $SW_{LoadDC} = OFF$ , depending on the connection or disconnection of loads to the DC bus, respectively.

3.1.2.9. DC Load Hysteresis ( $DC_{Load\_hyst}$ ). Parameter  $DC_{Load\_hyst}$  is calculated as 10% of the overall power consumed by the DC loads,  $DC_{Load\_hyst} = 01 \cdot P_{DCLoad}$ . This parameter acts as a hysteresis value for the comparison thresholds which produce the decisions of the MGCP, so that undesirable power transients are avoided.

3.1.2.10. Power consumed for the batteries to C10 ( $PESS_{C10}$ ). Parameter  $PESS_{C10}$  is the maximum power consumption for the charge of the batteries of the ESS,  $PESS_{C10} = (V_{Bat} \cdot I_{C10}) / \eta_{ESS}$ . It has been established that the batteries are charged with a current equal to  $I_{C10} = C10 / 10$ , being  $C10$  the specified battery capacity (measured in A·h) for a discharge time of 10 hours.

## 3.2. HY MG Management Algorithm

Several calculations and functions are necessary for the decision-making of the HY MG control algorithm. These calculations and functions depend on the SOC of the battery, the availability of power in the buses, the limits set at a higher level, and the status of  $SW_{LoadDC}$ .

3.2.1. Operation Functions the MGCP. The power management algorithm embedded in the MGCP executes 12 operation functions according to the various operating scenarios. The operation functions of the MGCP and their interactions with the converters of the MG are described in the following.

3.2.1.1. Operation Functions in DC Load Connection Mode ( $SW_{LoadDC} = ON$ ). *Function 1 (F1)*: Function F1 establishes that DC loads are fed. While  $SOC \leq SOC_{Full}$ , the DC-DC converter of the ESS charges the batteries from the DC bus with a current  $I_{C10}$ . The PV DGs work at their maximum power point (MPP), so that  $MPPT = ON$ . If there's not enough power available from the PV DGs connected to the DC bus, the ILC can extract the rest of the power from the AC bus with the only restriction:  $|\hat{P}_{ILC_{AC}}| \leq P_{ILC_{AC}-Rated}$ , taking into account that  $EDL = OFF$ .

Function 2 (F2): All DC loads are fed. While  $SOC \leq SOC_{Full}$ , the DC-DC converter of the ESS charges the batteries from the DC bus with a current equal to  $I_{C10}$ . The PV DGs work at their MPP ( $MPPT = ON$ ). In this case the PV DGs connected to the DC bus may produce an excess of power which can be injected to the AC bus by the ILC, with the only limitation of its rated power,  $\hat{P}_{ILC,AC} \leq P_{ILC,AC-Rated}$ , if is necessary.

Function 3 (F3): All DC loads are fed. While  $SOC \leq SOC_{Full}$ , the DC-DC converter of the ESS charges the batteries from the DC bus with a current equal to  $I_{C10}$ . The PV DGs don't work at their MPP ( $MPPT = OFF$ ). In this case the PV DGs connected to the DC bus produce a limited amount of power, because the power which can be injected to the AC bus by the ILC is limited by the grid operator. The power injected from the DC bus to the AC bus by the ILC is given by:  $P_{ILC,AC} \leq \hat{P}_{ILC,AC}|_{MG-to-Grid}$ . Figure 3 depicts the power dispatch inside the HY MG after applying the operation functions F3, F8, F10, and F11. Function 3 is shown in Figure 3(a).

Function 4 (F4): All DC loads are disconnected.  $SOC \leq SOC_{MIN}$ , the ESS is in standby mode. The flag  $SW_{LoadDC}$  changes from ON to OFF, entering the DC load disconnection mode. The PV DGs work at their MPP ( $MPPT = ON$ ).

Function 5 (F5): All DC loads are fed. While  $SOC \leq SOC_{Full}$ , the DC-DC converter of the ESS charges the batteries from the DC bus with a current equal to  $I_{C10}$ . The PV DGs work at their maximum power point ( $MPPT = ON$ ). The ILC injects the excess power at the DC bus to the AC bus. The power injected to the AC bus must comply:  $P_{ILC,AC} \leq \hat{P}_{ILC,AC}|_{MG-to-Grid}$ .

Function 6 (F6): All DC loads are fed. As the SOC has reached  $SOC_{Full}$ , the DC-DC converter of the ESS stops charging the batteries, setting the ESS in standby mode. The PV DGs work at their MPP ( $MPPT = ON$ ), producing an excess of power which can be injected to the AC bus by the ILC.

Function 7 (F7): All DC loads are fed. While  $SOC \leq SOC_{Full}$ , the DC-DC converter of the ESS charges the batteries from the DC bus with a current, whose value is shown by (10), which is smaller than  $I_{C10}$ . The PV DGs work at their MPP ( $MPPT = ON$ ). If there's not enough power available from the PV DGs, the ILC can extract the rest of power from the AC bus, subjected to the limit:  $|P_{ILC,AC}| \leq \hat{P}_{ILC,AC}|_{Grid-to-MG}$ .

$$I_{Chref} = MIN \left( I_{C10}, \frac{P_{AvailableDC\_MG} + \hat{P}_{ILC,AC}|_{Grid-to-MG}}{V_{DC}} \right) \quad (10)$$

Function 8 (F8): All DC loads are fed. While  $SOC \geq SOC_{MIN}$  the DC-DC converter of the ESS operates as a

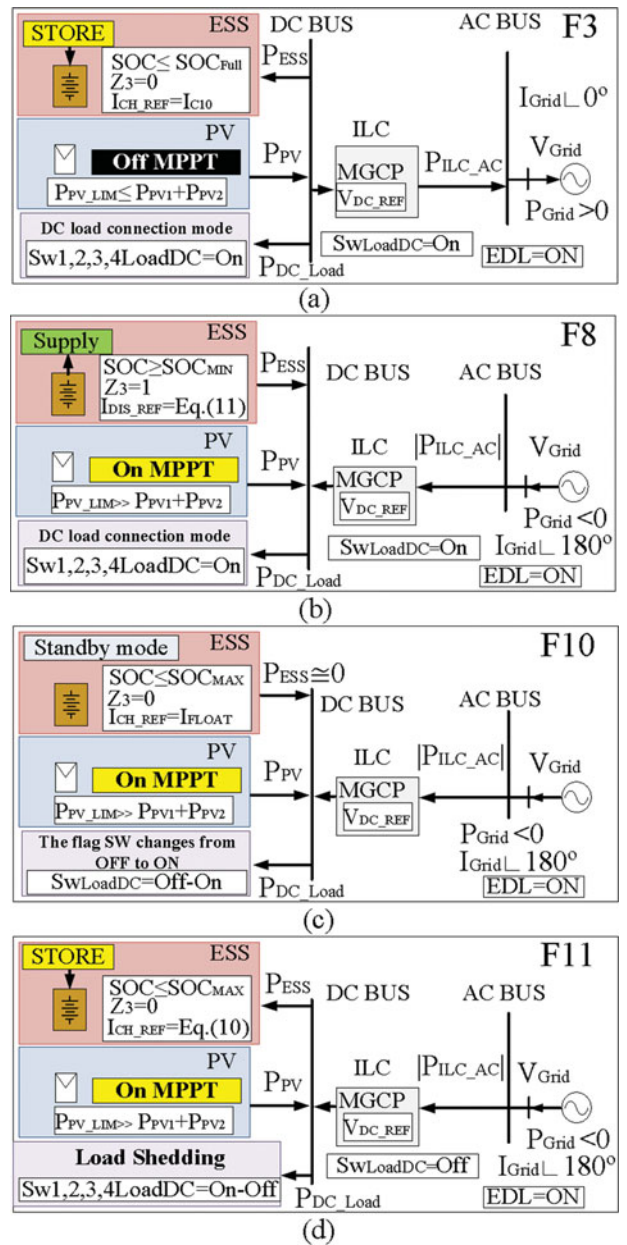


FIGURE 3. Power dispatch inside the HY MG after applying the operation functions: (a) Function 3, (b) Function 8, (c) Function 10, and (d) Function 11.

controlled current source discharging the batteries to the DC bus. In F8 the PV DGs work at their MPP ( $MPPT = ON$ ). The sum of the power coming from the ESS and from the PV DGs is not enough to energize the DC loads, so that the required extra power can be transferred from the AC bus to the DC bus through the ILC. That extra power is limited in order not to override the power which can be absorbed by the DC loads. Equation (11) shows the expression of the discharge current. In this case the extra available power is



negative ( $P_{AvailableDC\_MG} < 0$ ), because the power coming from the PV DGs is not enough to energize the DC loads, see Figure 3(b).

$$I_{Dis_{ref}} = MIN \left( I_{C10}, \left| \frac{P_{AvailableDC\_MG} + \hat{P}_{ILC_{AC}}|_{Grid-to-MG}}{V_{bat}} \right| \right) \quad (11)$$

**Function 9 (F9):** All DC loads are fed. As the SOC has reached  $SOC_{Full}$ , the DC-DC converter of the ESS stops charging the batteries, entering standby mode. The PV DGs don't work at their maximum power point ( $MPPT = OFF$ ), because the DC loads cannot absorb the sum of MPP powers. The ILC injects a limited amount of power from the DC bus to the AC bus, which is the required extra power to feed the DC loads.

**3.2.1.2 Operation Functions in DC Load Disconnection Mode ( $SW_{LoadDC} = OFF$ ).** **Function 10 (F10):** In F10 the flag  $SW_{LoadDC}$  switches from OFF to ON. All DC loads are fed. The ESS is in standby mode. The PV DGs work at their MPP ( $MPPT = ON$ ), function 10 is shown in Figure 3(c).

**Function 11 (F11):** Only some DC loads are fed (load shedding). This function selects the overall amount of power consumed by the DC loads. F11 offers the ability to turn on and turn off each of the DC loads automatically. While  $SOC \leq SOC_{MAX}$ , the DC-DC converter of the ESS charges the batteries with a current smaller than  $I_{C10}$ , given by (10). The PV DGs work at their MPP ( $MPPT = ON$ ), function 11 is shown in Figure 3(d).

Equation (12) gives the expression of  $Cal.0$ , which is the calculation of the available PV power plus the maximum power that can be transferred from the AC bus to the DC bus by the ILC. A decision tree can be observed in Figure 4, which depicts how 1 to 4 DC-loads are connected-disconnected as a function of the value of  $Cal.0$ . If  $Cal.0$  is not enough to energize all the DC loads, F11 begins their disconnection depending on the values of  $Cal.0$  and of the state (1 or 0) of the logic variables  $Comp.1$  to  $Comp.3$ , which are calculated as OR functions. Note that a 10% hysteresis band of the power of one DC load has been chosen for establishing the comparison thresholds:  $DC_{Load\_hyst} = 0.1 \cdot 2 \text{ kW} = 200 \text{ W}$ .

$$Cal.0 = P_{PV} + \hat{P}_{ILC_{AC}}|_{Grid-to-MG}. \quad (12)$$

**Function 12 (F12):** All DC loads are fed. While  $SOC \leq SOC_{MAX}$ , the DC-DC converter of the ESS charges the batteries with a current smaller than  $I_{C10}$ , given by (10). The DGs work at their MPP ( $MPPT = ON$ ). If the power coming from the PV DGs is not enough to energize the DC loads, the required extra power can be transferred from the AC bus to the DC bus through the ILC.

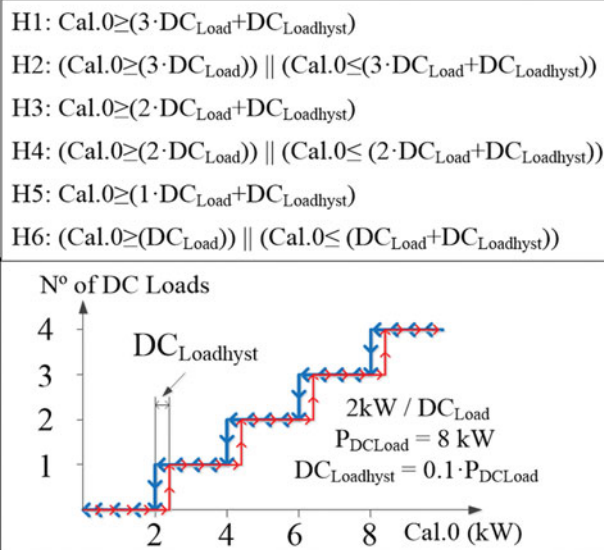
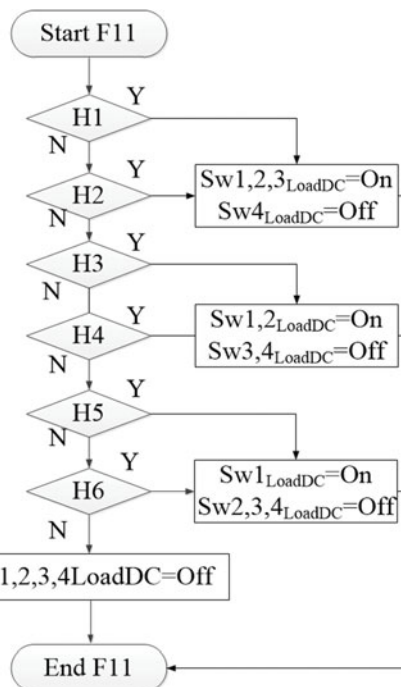
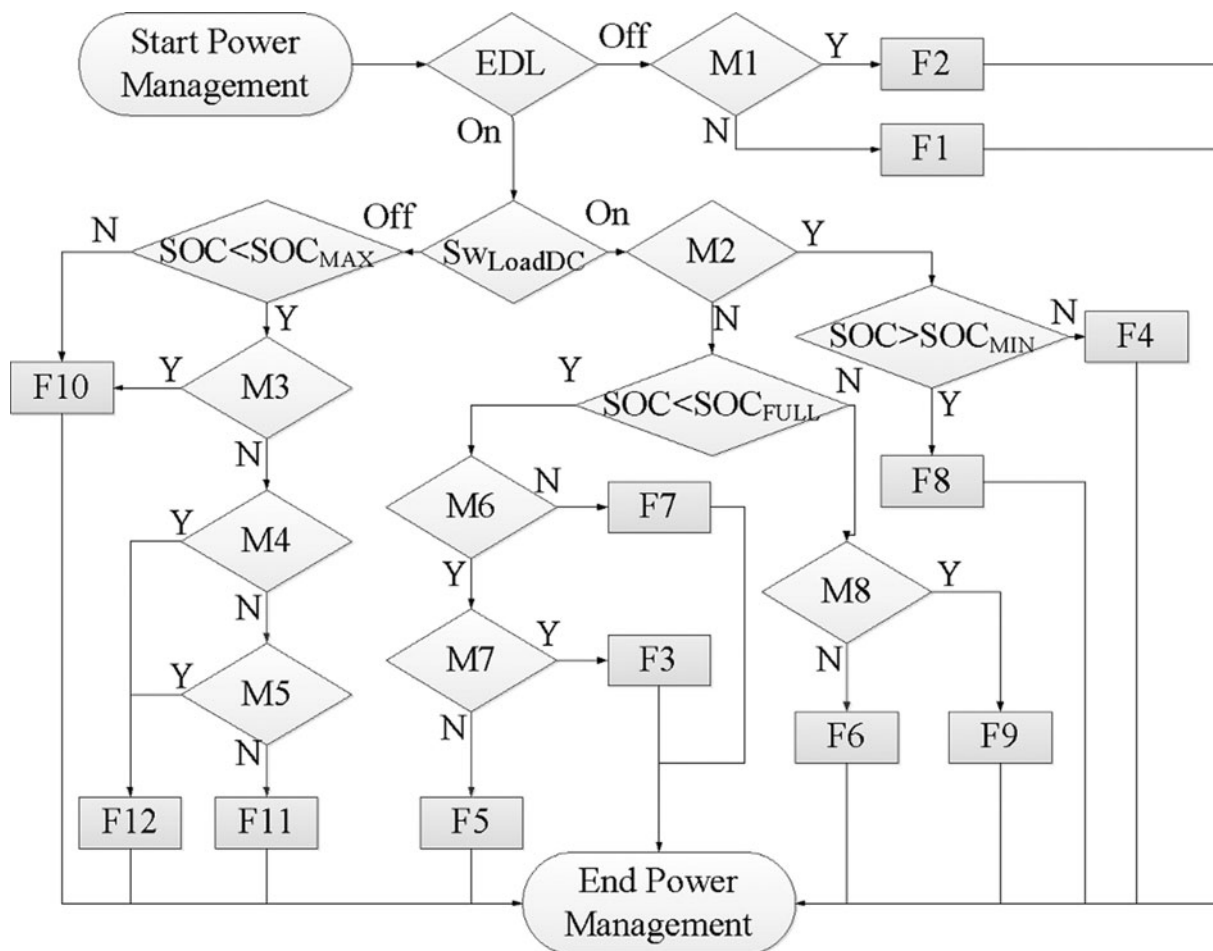


FIGURE 4. DC load shedding function.

### 3.2.2. Power Management Algorithm of the HY MG.

Figure 5 depicts the flowchart of the proposed HY MG power management algorithm,  $Comp.4$  is a logic variable which is calculated as an OR function. The DC load switch flag,  $SW_{LoadDC}$ , and the flag  $EDL$ , are fundamental parameters for decision-making. When  $EDL = Off$ , there is no energy dispatch limit, so that functions F1 or F2 can be applied. When  $EDL = On$  and  $SW_{LoadDC} = ON$ , the MGCP applies functions F3 to F9. The flag  $SW_{LoadDC}$  can be turned off by F4,



- M1:  $P_{\text{AvailableDCMG}} > 0$
- M2:  $\text{Cal.1} > DC_{\text{Loadhyst}}$
- M3:  $\text{Cal.3} > DC_{\text{Loadhyst}}$
- M4:  $\text{Cal.0} \geq P_{\text{DCLoad}}$
- M5:  $\text{Cal.0} \leq (P_{\text{DCLoad}} + DC_{\text{Loadhyst}})$
- M6:  $\text{Cal.1} > PESS_{C10}$
- M7:  $P_{\text{AvailableDCMG}} > \text{Cal.2}$
- M8:  $P_{\text{AvailableDCMG}} > P_{\text{ILCAC|MG-to-Grid}}$

FIGURE 5. Power management algorithm of the HY MG.

after which the MGCP can apply functions F10 to F12. The functions are implemented so that the power transfer limits between both buses are not exceeded. The basic calculations performed by the power management algorithm, *Cal.0* to *Cal.4*, are shown by (12) to (15), and allow checking the

power availability of both buses, taking into account their power dispatch limits. Equation (13) stands for the power availability in the DC bus, coming from DGs and batteries, plus the maximum power which can be extracted from the AC bus to the DC bus.

$$Cal.1 = P_{Available_{DCMG}} + \hat{P}_{ILC_{AC}}|_{Grid-to-MG} \quad (13)$$

Equation (14) stands for the maximum power which can be injected from the DC bus to the AC bus plus the power consumed for charging the batteries at a current  $I_{C10}$ .

$$Cal.2 = \hat{P}_{ILC_{AC}}|_{MG-to-Grid} + P_{ESS_{C10}} \quad (14)$$

In Eq. (15) the maximum power consumed by the DC loads is extracted from the PV power generated at the DC bus plus the maximum power which can be extracted from the AC bus to the DC bus.

$$Cal.3 = P_{PV} + \hat{P}_{ILC_{AC}}|_{Grid-to-MG} - \hat{P}_{DC_{Load}} \quad (15)$$

## 4. SIMULATION AND EXPERIMENTAL RESULTS AND DISCUSSION

### 4.1. Simulation Results

The proposed power management algorithm has been simulated by means of PSIM<sup>TM</sup> [22] under various scenarios. This study is focused in the particular case that the MG is operating in grid connected mode. The characteristics of the power electronic converters composing the MG are listed in Table 3. The simulation scenarios of the MG are explained in Table 4. It is supposed that the ESS is initially discharged ( $SOC \leq SOC_{MIN}$ ). A selected number of possible scenarios has been studied in order to demonstrate the suitable behavior of the HY MG in its most common and critical situations. In the scenarios under study step changes of the irradiation,

of the DC load and of the EDL are considered, as it can be observed from Table 4. The behavior of the proposed algorithm and the application of particular functions F1 to F12 by the MGCP can be observed from the following graphs. Figure 6 depicts the behavior of the currents  $I_{Bat}$ ,  $I_{PV} = I_{PV1} + I_{PV2}$  and of the SOC with time. The evolution of the powers  $P_{Bat}$ ,  $P_{PV}$ ,  $P_{DC_{Load}}$ ,  $P_{ILC_{AC}}$ , and  $P_{Grid}$  can be observed from Figure 7. Figure 8 provides a detail of the strongest transient of  $I_{ILC_{AC}}$ ,  $V_{DC}$ , and  $P_{ILC_{AC}}$  which takes place in the whole simulation, corresponding to the time span 34.8 s to 35.4 s. The analysis is performed according to the following time intervals:

Interval 1 ( $0 \leq t \leq 1$  s): This interval is divided into 2 subintervals.

$0 \leq t < 40$  ms: At  $t = 0$  s the ESS is initially discharged ( $SOC \leq SOC_{MIN}$ ). The irradiation is  $300$  W/m<sup>2</sup> and the overall DC load absorbs 8 kW. Due to the fact that the PV available power,  $P_{PV}$ , at that low irradiation level is not enough to feed the loads, the MGCP applies function F4, internally activating flag  $SW_{LoadDC} = OFF$ .

$40$  ms  $\leq t < 1$  s: After to F4, F11 is applied to disconnect two DC loads (overall DC load = 4 kW) and the batteries are charged with a current given by (10).

Interval 2 ( $1$  s  $\leq t \leq 10$  s): At  $t = 1$  s the irradiation undergoes a change from  $300$  W/m<sup>2</sup> to  $600$  W/m<sup>2</sup>, whereas the SOC keeps growing below  $SOC_{MAX}$ . The MGCP goes on applying F11. The PV generation is increased, and F11 connects an additional 2 kW DC load (overall DC load = 6 kW) to the DC bus. The MGCP makes both PV DC-DC converters to operate at their MPP, whereas the DC bus voltage is regulated to 420 V by the ILC.

Interval 3 ( $10$  s  $\leq t \leq 18$  s): This interval is divided into 5 subintervals.

$10 \leq t < 10.2$  s: At  $t = 10$  s the irradiation decreases from  $600$  W/m<sup>2</sup> to  $400$  W/m<sup>2</sup>, whereas the SOC keeps growing below  $SOC_{MAX}$ . The MGCP maintains F11. The power generated by the panels  $P_{PV}$  with this irradiation is insufficient to feed three loads and F11 disconnects one load (DC load = 4 kW) in the DC bus. This is shown in Figure 6.

$10.2$  s  $\leq t < 10.24$  s: At  $t = 10.2$  s the SOC surpasses  $SOC_{MAX}$ , whereas the irradiation stays at a constant value of  $400$  W/m<sup>2</sup>. The MGCP applies F10 after detection of  $SOC_{MAX}$ , which internally activates the flag  $SW_{LoadDC} = ON$ .

$10.24$  s  $\leq t < 15.4$  s: At  $t = 10.24$  s the generated PV power at the current irradiation level is not enough to feed all the DC loads, so that the MGCP applies F8 in order to get additional power from the ESS, and the battery bank is discharged at a current given by (11). F8 connecting all DC loads (8 kW) to the DC bus and extracts power from the AC bus taking into

ILC	2 PV DC-DC converters (DGs)		ESS
$P_{ILC} = 10$ kW	$P_{PV\_BOOST} = 5$ kW	$P_{ESS\_HB} = 3$ kW	
$V_{Grid} = 230$ V	$V_{PV} = 306$ V	$V_{Bat} = 216$ V	
$F_{Grid} = 50$ Hz	$F_{SW\_PV} = 16$ kHz	$F_{SW\_ESS} = 16$ kHz	
$V_{DC} = 420$ V	$C_{OPV} = 1$ mF	$C_{iBat} = 1$ mF	
$F_{SW\_ILC} = 12.8$ kHz	$C_{iPV} = 1$ mF	$C_{OBat} = 1$ mF	
$C_{DC} = 3.8$ mF	$L_{PV} = 5.4$ mH	$L_{Bat} = 5.4$ mH	
$L1 = 1.8$ mH	<b>PV Panel: Atersa</b>	<b>Battery Bank: SUN</b>	
$L2 = 0.4$ mH	<b>A-250P GSE</b>	<b>POWER VRM</b>	
$C = 2$ $\mu$ F	$V_{PV\_OC} = 37.61$ V	<b>12V105</b>	
$C_{DC} = 3.8$ mF	$I_{PV\_MAX} = 8.18$ A	$V_{Bat\_NOM} = 12$ V	
	$V_{PV\_MAX} = 30.58$ V	$V_{Bat\_MIN} = 10.28$ V	
	$I_{PV\_CC} = 8.71$ A	$V_{Bat\_MAX} = 14.1$ V	
		$C_{10} = 105$ A·h	
		$I_{C10} = 10.5$ A	

**TABLE 3.** Characteristics of the power converters conforming the HY MG.

**SIMULATION scenarios <sup>(1)</sup>**

	Time intervals (s)						
<b>Time interval number</b>	1	2	3	4	5	6	7
<b>Time span (s)</b>	$0 < t < 1$	$1 < t < 10$	$10 < t < 18$	$18 < t < 20$	$20 < t < 28$	$28 < t < 35$	$35 < t < 40$
<b>Irradiation (W/m<sup>2</sup>)</b>	300	600	400	800	800	800	100
<b>Load connected at the DC bus</b>	4 loads (8 kW)	4 loads (8 kW)	4 loads (8 kW)	4 loads (8 kW)	2 loads (4 kW)	2 loads (4 kW)	2 loads (4 kW)
<b>EDL</b>	On	On	On	On	On	Off	Off
<b>ILC</b>	The HY MG is operating in grid-connection mode						
<b>ESS</b>	The batteries of the ESS are initially discharged. $SOC \leq SOC_{MIN}$						
<b>Power limits</b>	$P_{MG-to-Grid} = 4 \text{ kW}$ , $P_{Grid-to-MG} = 1 \text{ kW}$ , $P_{DC\_LOAD} = 8 \text{ kW}$						
<b>AC MG</b>	$P_{AC\_DG} = 5 \text{ kW}$ , $P_{AC\_LOAD} = 4 \text{ kW}$						

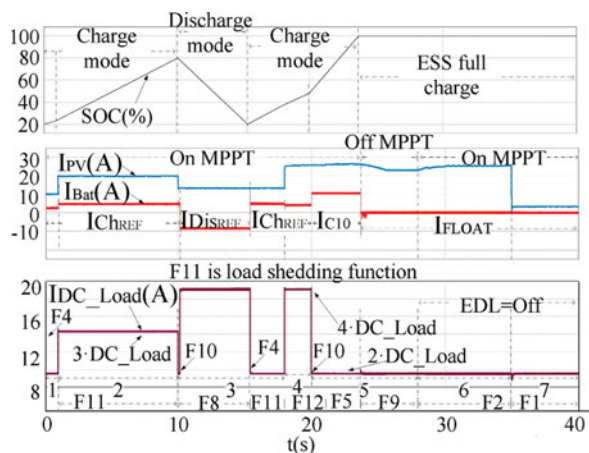
<sup>(1)</sup> It's worth pointing out that step changes of irradiation not correspond to reality, but they allow studying the behavior of the HY MG and the stability of the buses in the worst cases. In order to check of the proposed algorithm in different situations and for a short time period, in this work the algorithm is running in simulations at 25 Hz. The duration of operation functions F4 and F10 is one clock cycle (40 ms), because their main function is to change the load shedding function.

**EXPERIMENTAL scenarios**

<b>ESS</b>	Experiment 1: The batteries of the ESS are initially charged. $SOC = SOC_{MAX}$				
<b>Time span (s)</b>	$0 < t < 8$	$8 < t < 11$	$11 < t < 41$	$41 < t < 44$	$44 < t < 50$
<b>Irradiation (W/m<sup>2</sup>)</b>	100	100 to 800	800	800 to 100	100
<b>ESS</b>	Experiment 2: The batteries of the ESS are initially discharged. $SOC \leq SOC_{MIN}$				
<b>Time span (s)</b>	$0 < t < 7$	$7 < t < 10$	$10 < t < 40$	$40 < t < 43$	$43 < t < 50$
<b>Irradiation (W/m<sup>2</sup>)</b>	100	100 to 800	800	800 to 100	100
<b>DC Load connected</b>	4 loads (2.4 kW)				
<b>EDL</b>	On				
<b>ILC</b>	The HY MG is operating in grid-connection mode				
<b>Power limits</b>	$P_{MG-to-Grid} = 4 \text{ kW}$ , $P_{Grid-to-MG} = 1 \text{ kW}$ , $P_{DC\_LOAD} = 2.4 \text{ kW}$				
<b>AC MG</b>	$P_{AC\_DG} = 5 \text{ kW}$ , $P_{AC\_LOAD} = 4 \text{ kW}$				

**TABLE 4.** Possible scenarios of the HY MG.

account the limit the maximum power that can be extracted of the same  $|P_{ILCAC}| \leq \hat{P}_{ILCAC}|_{Grid-to-MG}$ , and the ESS injects the current required by the DC bus to feed the DC loads.


**FIGURE 6.** Evolution of the currents of the HY MG and of the SOC of the batteries.

$15.4 \text{ s} \leq t < 15.44 \text{ s}$ : At  $t = 15.4 \text{ s}$  the SOC goes below  $SOC_{MIN}$ , so that the MGCP applies F4, internally activating 495 flag  $SW_{LoadDC} = OFF$ .

$15.44 \text{ s} \leq t < 18 \text{ s}$ : At  $t = 15.44 \text{ s}$  the MGCP applies F11. F11 disconnects two DC loads (overall  $DC \text{ load} = 4 \text{ kW}$ ), so that the batteries are charged with a current given by (10).

Interval 4 ( $18 \text{ s} \leq t \leq 20 \text{ s}$ ): At  $t = 18 \text{ s}$  the irradiation 500 undergoes a linear change of  $400 \text{ W/m}^2$  to  $800 \text{ W/m}^2$ , being  $SOC < SOC_{MAX}$ . The generated PV power and the power extracted from the AC bus are enough to feed all DC loads. Due to limitations on the amount of power that can be inter- 505 changed between the buses, the MGCP applies F12 and the batteries are charged with a current given by (10). F12 connects all the DC loads and also sets the PV sources at their MPP.

Interval 5 ( $20 \text{ s} \leq t \leq 28 \text{ s}$ ): This interval is divided into 3 510 subintervals.

$20 \leq t < 20.04 \text{ s}$ : The irradiation keeps a constant  $800 \text{ W/m}^2$  value, whereas SOC remains below  $SOC_{Full}$ . At  $t = 20 \text{ s}$  the load connected to the DC bus decreases from  $8 \text{ kW}$  to



4 kW. The PV generated power ( $P_{PV}$ ) at the current irradiation is enough to feed all DC loads. The MGCP applies F10 which internally activates the flag  $SW_{LoadDC} = ON$ .

20.04 ≤ t < 23.7 s: At t = 20.04 s MGCP applies F5. F5 sets the charge the batteries with a current  $I_{C10}$ . The PV sources work at their MPP. The ILC injects the power excess to the AC bus.

23.7 s ≤ t < 28 s: Both the irradiation (800 W/m<sup>2</sup>) and the DC load (4 kW) remain constant, whereas the SOC has reached 100%. The power generated by the panels is higher than that necessary for feeding the DC loads,  $P_{PV} > 4 kW$ . The MGCP applies F9 to stop charging the batteries and to set the PV generators outside their MPP ( $MPPT = OFF$ ). In this case:  $P_{ILC_{AC}} \leq \hat{P}_{ILC_{AC}}|_{MG-to-Grid}$ .

Interval 6 (28 s ≤ t ≤ 35 s): The irradiation and the SOC remain constant, 800 W/m<sup>2</sup> and 100%, respectively. EDL switches from On to Off. The MGCP applies F2 and the ILC injects power to the grid to its rated power if is necessary,  $P_{ILC_{AC}} \leq P_{ILC_{AC-Rated}}$ . At t = 30 s MPPT switches from OFF to ON.

Interval 7 (35 s ≤ t ≤ 40 s): The irradiation undergoes a change of 800 W/m<sup>2</sup> to 100 W/m<sup>2</sup>. The MGCP applies F1, so that the ILC can extract power from the grid,  $|P_{ILC_{AC}}| \leq P_{ILC_{AC-Rated}}$ .  $MPPT = ON$ .

In Figure 7 the power exchange between devices of the MG is shown. In the first part of interval 5 (20 < t < 23.7 s) the

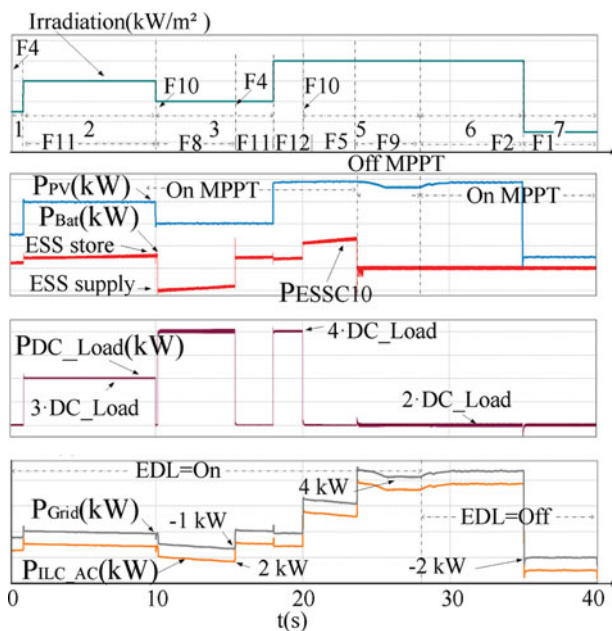


FIGURE 7. Evolution of the power exchange at the HY MG and irradiation.

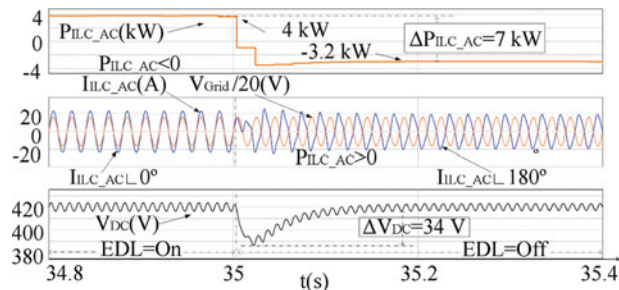


FIGURE 8. Detail of the strongest transient of  $I_{ILC_{AC}}$ ,  $V_{Grid}$ ,  $V_{DC}$ , and  $P_{ILC_{AC}}$ , which takes place in interval 7.

MGCP makes that the battery system is charged to its maximum capacity,  $P_{ESS_{C10}}$ , using the power available from the PV DGs. In the second part of interval 5 (23.7 s ≤ t < 28 s) the MGCP limits the generation from the PV DGs, setting their operation point out of the MPP ( $MPPT = OFF$ ).

The ILC is responsible for controlling the voltage of the DC bus, because the AC bus works in grid connection mode. The ILC also carries out the synchronization of the AC bus with the grid, achieving that the current  $I_{ILC_{AC}}$  flowing through the ILC to the AC bus is low distorted and in phase with the grid voltage,  $V_{Grid}$ , when the MG exports power to the grid or in phase opposition when the MG imports power from the grid. Figure 8 shows the waveforms of  $I_{ILC_{AC}}$  and of  $V_{Grid}$  in both situations, where a smooth transient, good synchronization and a low distortion of  $I_{ILC_{AC}}$  can be observed in the transition from exporting to importing power to/from the AC bus. A smooth transient of the DC bus voltage,  $V_{DC}$ , is also observed in that transition at t = 35s, which is the strongest transient of the DC bus during the whole study, consisting of a transient under-voltage of  $\hat{V}_{DC} = 34V$ , less than 10% of the DC bus voltage. It should be considered that the power,  $P_{ILC_{AC}}$ , interchanged between the ILC and the AC bus at t = 35 s undergoes an abrupt change from 3.8 kW to -3.2 kW (7 kW step), provoked by a fast irradiation decrease.

## 4.2. Experimental Results

Several experimental power electronic converters, whose characteristics are summarized in Table 3, have been built for validating the proposed power management algorithm. The following devices have been connected to the DC bus of the HY MG available in the lab: a 3 kW battery ESS, a 2.5 kW PV source and four electronic switches to connect/disconnect four DC loads of 600 W each one ( $\hat{P}_{DC_{Load}} = 2.4kW$ ). Figure 9 shows a picture of the experimental setup. The batteries have been emulated by a bidirectional DC source/battery emulator model TC.GSS-Bidirectional-DC-PSU from Regatron. The



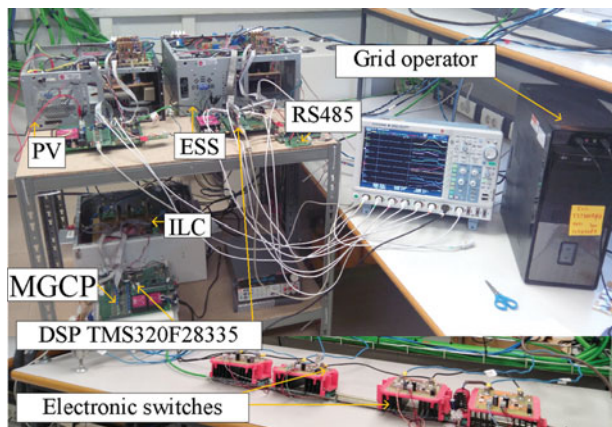


FIGURE 9. Experimental setup picture.

575 PV array has been emulated by means of a 10 kW PV array simulator TerraSAS ETS1000/10 from Ametek. Three experiments have been carried out. The experimental scenarios are summarized by Table 4. Figures 10 and 11 depict the waveforms of the currents, voltages, and powers of the power converters of the DC bus of the MG, corresponding to Figure 10, experiment 1 and Figure 11, experiment 2. Figure 12 correspond to the experiment 3.

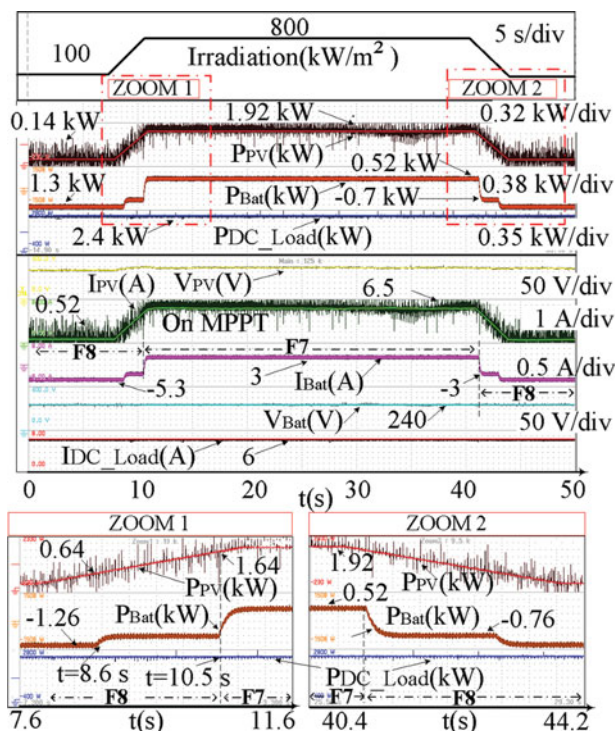


FIGURE 10. Experiment 1: Evolution of the currents, voltages, and the power exchange in the HY MG.

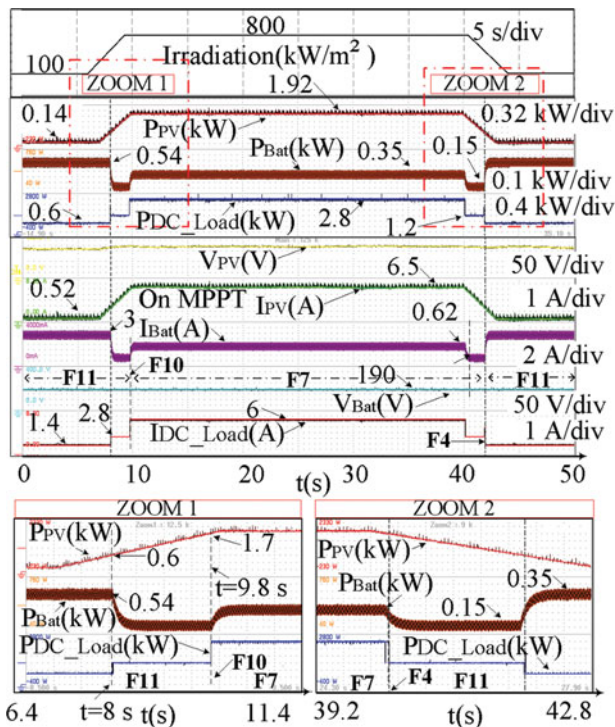


FIGURE 11. Experiment 2: Evolution of the currents, voltages, and the power exchange in the HY MG.

Experiment 1 and experiment 2 show the behavior of the system with the same change of the irradiation level at the PV source, but with a different SOC of the ESS. The available power injected from the AC bus to the DC bus by the ILC is  $P_{ILC\_DC} = -1 \text{ kW}$ .

Experiment 1: The ESS is initially at an  $SOC \geq 80\%$  (charged). In Figure 1 can be observed that the four loads keep connected during the whole experiment. ( $P_{DC\_Load} = 2.4 \text{ kW}$ ).

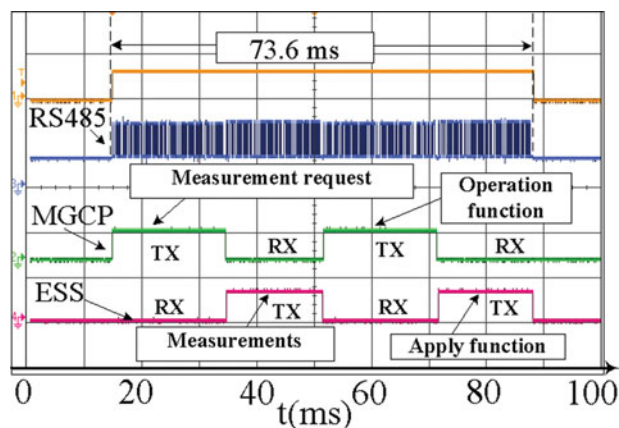


FIGURE 12. Experiment 3: Computing time of the communication between the MGCP and one of the microgrid elements.

The hysteresis level for comparisons with thresholds is:  
 $DC_{Load\_hyst} = 240 W$ .

*Interval 1* ( $0 s \leq t \leq 8 s$ ): The irradiation level is  $100 W/m^2$  and the PV source works at its maximum power point (MPP), providing  $P_{PV} = 140 W$  to the DC bus. That irradiation is not enough to feed all the loads. Taking into account that the ESS is charged ( $SOC \geq 80\%$ ) the MGCP transfers the maximum possible power from the AC bus ( $P_{ILC\_DC} = -1 kW$ ) to the DC bus through the ILC and applies F8. F8 keeps all the DC loads connected and orders the ESS supplying all the power required by the DC bus,  $P_{Bat} = -1.26 kW$ .

*Interval 2* ( $8 s \leq t \leq 11 s$ ): The irradiation increases from  $100 W/m^2$  to  $800 W/m^2$  in 3 s. The MGCP keeps F8 activated and the power delivered by the ESS can be reduced.

At  $t = 8.6 s$ ; MGCP detects increasing generation, the PV source works at its MPP delivering  $P_{PV} = 640 W$ . The MGCP keeps F8 activated and transfers the maximum possible power from the AC bus ( $P_{ILC\_DC} = -1 kW$ ), and keeps all the DC loads connected. ESS supplying all the power required by the DC bus, the power delivered by the ESS is reduced to  $P_{Bat} = -0.76 kW$ .

At  $t = 10.5 s$  the PV source works at its MPP delivering  $P_{PV} = 1640 W$ , being  $P_{ILC\_DC} = -1 kW$ . In this moment the MGCP detects that the available power at the DC bus to feed all the DC loads is higher than the hysteresis level ( $Cal.1 > DC_{Load\_hyst}$ ). The MGCP changes from F8 to F7. F7 forces the ESS to change its operation to energy storage mode, the batteries are charged with a current given by (10). The MGCP changes the set-point of the ESS charge current  $I_{Ch\_ref}$ , until the available power generation is stable (At  $t = 11.6 s$ ,  $P_{Bat} = 0.5 kW$ ).

**Experiment 2:** The ESS is initially at an  $SOC \leq 20\%$  (discharged).

*Interval 1* ( $0 s \leq t \leq 7 s$ ): The irradiation level is  $100 W/m^2$  and the PV source works at its maximum power point (MPP), providing  $P_{PV} = 140 W$  to the DC bus. That irradiation is not enough to feed all the loads. Considering that the ESS is discharged ( $SOC < 20\%$ ), the MGCP transfers the maximum possible power from the AC bus ( $P_{ILC\_DC} = -1 kW$ ) to the DC bus through the ILC, and applies the load shedding function F11. Taking into account that the available power at the DC bus ( $1140 W$ ) is not enough to feed two loads, F11 connects only one DC load ( $600 W$ ). The rest of the available power is used for charging the batteries at  $P_{Bat} = 540 W$ .

*Interval 2* ( $7 s \leq t \leq 10 s$ ): The irradiation increases from  $100 W/m^2$  to  $800 W/m^2$  in 3 s. The MGCP keeps function F11 activated.

At  $t = 8 s$  the PV source works at its MPP delivering  $P_{PV} = 600 W$ , whereas  $P_{ILC\_DC} = -1 kW$ . At this moment the MGCP detects that the available power at the DC bus taking into account the hysteresis level is enough to feed two of the loads. F11 connects two loads and changes the set-point  $I_{Ch\_ref}$  of the ESS from 2.9 A to 0.78 A, being  $P_{Bat} = 150 W$ . Note that at  $t = 8 s$ , after the connection of the two loads, only  $|P_{ILC\_DC}| \leq 0.75 kW$  is taken from the AC bus. This ensures a minimum level of power available in the DC bus.

At  $t = 9.8 s$ , the PV source works at its MPP delivering  $P_{PV} = 1700 W$ , being  $P_{ILC\_DC} = -1 kW$ . At this moment the MGCP detects that the available power at the DC bus to feed all the DC loads is greater than the hysteresis level ( $DC_{Load\_hyst}$ ). The MGCP applies function F10 which internally activates the flag  $SW_{LoadDC} = ON$ . After that the MGCP starts a transition from F10 to F7. F7 connects all the DC loads and changes the set-point of the ESS,  $I_{Ch\_ref} = 1.82 A$  until the available power generation is stable at the instant  $t = 11.4 s$ , being  $P_{Bat} = 0.35 kW$ . At  $t = 9.8 s$  the MGCP applies function F10 during an execution cycle of the algorithm, i.e. during 73 ms. After that, function F7 is applied. In the zoom areas of Figures 10 and 11 the power flow between the generators and the loads can be observed. No oscillations in the transients are observed, which could point out any instability problem.

**Experiment 3:** The operation functions broadcasted by the MGCP to the MG elements have a communications delay which depends on the RS485 communication system. In the experimental MG the computing time of one operation function and its delay to be broadcasted and processed by one of the elements is lower than 74 ms, as it can be observed in Figure 12.

## 5. CONCLUSIONS

A new power management algorithm for the efficient coordination of the power converters composing a hybrid microgrid working in grid-connected mode is presented. The algorithm is programed in a Microgrid Central Processor and it is based on grouping the devices together according to their type: generation, storage, interlinking converter and load. The algorithm selects the suitable configuration of the microgrid among a set of several predefined functions, which establish the configuration of each of the devices in every plausible scenario of the MG. In this paper 12 operations functions have been defined, but that number could be extended. The choice of the functions to be applied depends on the status of the distributed generators, the loads, the energy storage and the energy dispatch limit between the AC and DC buses

established by the grid operator. The operations functions are the set-points that define the status of each converter, and are broadcasted by the MGCP through a low bandwidth RS485 communications system. The experimental and simulation results confirm that the proposed power management algorithm allows a suitable power balance among the HY MG devices at changes of the irradiance, of the load and of the state of charge of the ESS, complying with the power dispatch limit set by the public grid operator.

## FUNDING

This work has been cofinanced by the Spanish Ministry of Economy and Competitiveness (MINECO) and by the European Regional Development Fund (ERDF) under Grant ENE2015-64087-C2-2.

## ORCID

Robert Salas-Puente  <http://orcid.org/0000-0001-6514-3318>

## REFERENCES

- [1] G. de J. Roa-Escalante, J. M. Sánchez-Lozano, J.-G. Faxas, M. S. García-Cascales, and A. Urbina, "The effects of photovoltaic electricity injection into microgrids: Combination of Geographical Information Systems, multicriteria decision methods and electronic control modeling," *Energy Convers. Manage.* vol. 96, pp. 88–99, 2015. DOI: 10.1016/j.enconman.2015.02.060.
- [2] I. Kougias, S. Szabo, F. Monforti-Ferrario, T. Huld, and K. Bodis, "A methodology for optimization of the complementarity between small-hydropower plants and solar PV systems," *Renewable Energy*. vol. 87, pp. 1023–1030, 2016. DOI: 10.1016/j.renene.2015.09.073.
- [3] C. Adel, B. Djamel, B. C. Said, and B. Jean-Michel, "A local energy management of a hybrid PV-storage based distributed generation for microgrids," *Energy Convers. Manage.* vol. 90, pp. 21–33, 2015. DOI: 10.1016/j.enconman.2014.10.067.
- [4] K.-K. Sam and R. N. Abd, "Coordinated control of smart microgrid during and after islanding operation to prevent under frequency load shedding using energy storage system," *Energy Convers. Manage.* vol. 127, pp. 623–646, 2016. DOI: 10.1016/j.enconman.2016.09.052.
- [5] F. Katiraei and M. R. Iravani, "Power management strategies for a microgrid with multiple distributed generation units," *IEEE Trans. Power Syst.* vol. 21, pp. 1821–1831, 2006. DOI: 10.1109/TPWRS.2006.879260.
- [6] M. Sechilariu, B. C. Wang, F. Locment, and A. Jouglet, "DC microgrid power flow optimization by multi-layer supervision control. Design and experimental validation," *Energy Convers. Manage.* vol. 82, pp. 1–10, 2014. DOI: 10.1016/j.enconman.2014.03.010.
- [7] N. Eghtedarpour and E. Farjah, "Control strategy for distributed integration of photovoltaic and energy storage systems in DC micro-grids," *Renewable Energy*. vol. 45, pp. 96–110, 2012. DOI: 10.1016/j.renene.2012.02.017.
- [8] A. A. Memon and K. Kauhaniemi, "A critical review of AC Microgrid protection issues and available solutions," *Electric Power Syst. Res.* vol. 129, pp. 23–31, 2015. DOI: 10.1016/j.epsr.2015.07.006.
- [9] X. Liu, P. Wang, and P. C. Loh, "A hybrid AC/DC micro-grid," *2010 Conf. Proc. IPEC*, Singapore, pp. 746–751, 2010.
- [10] P. Wang, X. Liu, C. Jin, P. Loh, and F. Choo, "A hybrid AC/DC micro-grid architecture, operation and control," *2011 IEEE Power Energy Soc. Gen. Meet.*, San Diego, CA, pp. 1–8, 2011.
- [11] J. V. Josep Guerrero, "Hierarchical control of droop-controlled AC and DC microgrids. A general approach toward standardization," *IEEE Trans. Ind. Electron.* vol. 58, pp. 158–172, 2011. DOI: 10.1109/TIE.2010.2066534.
- [12] X. Liu, P. Wang, Member and P. C. Loh, "A hybrid AC/DC microgrid and coordination control," *IEEE Trans. Smart Grid*. vol. 2, pp. 278–286, 2013.
- [13] F. Nejjabatkhah and Y. W. Li, "Overview of power management strategies of hybrid AC/DC microgrid," *IEEE Trans. Power Electron.* vol. 30, pp. 7072–7089, 2015. DOI: 10.1109/TPEL.2014.2384999.
- [14] S. M. Poh Chiang Loh, "Autonomous control of interlinking converter with energy storage in hybrid AC–DC microgrid," *IEEE Trans. Ind. Appl.* vol. 49, pp. 1374–1376, 2013. DOI: 10.1109/TIA.2013.2252319.
- [15] K. De Brabandere, et al., "A voltage and frequency droop control method for parallel inverters," in *IEEE Trans. Power Electron.* vol. 22, no. 4, pp. 1107–1115, July 2007. DOI: 10.1109/TPEL.2007.900456.
- [16] P. C. Loh, D. Li, Y. K. Chai, and F. Blaabjerg, "Autonomous operation of hybrid microgrid with AC and DC subgrids," *IEEE Trans. Power Electron.* vol. 28, pp. 2214–2223, 2013. DOI: 10.1109/TPEL.2012.2214792.
- [17] F. Luo, K. H. Loo, and Y. M. Lai, "A hybrid AC/DC microgrid control scheme with voltage-source inverter-controlled interlinking converters," *2016 18th Eur. Conf. Power Electron. Appl. (EPE'16 ECCE Europe)*, Karlsruhe, pp. 1–8, 2016.
- [18] Y. Karimi, J. M. Guerrero, and H. Oraee, "Decentralized method for load sharing and power management in a hybrid single/three-phase islanded microgrid consisting of hybrid source PV/battery units," *2016 IEEE Energy Convers. Congr. Exposition (ECCE)*, Milwaukee, WI, USA, pp. 1–8, 2016.
- [19] M. A. Hasan, N. K. Vemula, and S. K. Parida, "Cost based dynamic load dispatch for an autonomous parallel converter hybrid AC-DC microgrid," *2016 Nat. Power Syst. Conf. (NPSC)*, Bhubaneswar, India, pp. 1–5, 2016.
- [20] MODBUS APPLICATION PROTOCOL SPECIFICATION V1.1b. [http://www.modbus.org/docs/Modbus\\_Application\\_Protocol\\_V1\\_1b.pdf](http://www.modbus.org/docs/Modbus_Application_Protocol_V1_1b.pdf)
- [21] S. Kenner, R. Thaler, M. Kucera, K. Volbert, and T. Waas, "Smart Grid architecture for monitoring and analyzing, including modbus and REST performance comparison," *2015 12th Int. Workshop Intell. Solut. Embedded Syst. (WISES)*, Ancona, pp. 91–96, 2015.
- [22] PowerSim. PSIM7.0. 2006.



## BIOGRAPHIES

**Robert Salas-Puente** was born in Merida, Venezuela, in 1981. He received the Ingeniero Electricista degree, in 2008 from the Universidad de Los Andes (ULA), Venezuela. He received the Ingeniería de Sistemas Electrónicos (M.Sc.) degree in 2015, from the Universitat Politècnica de València (UPV), Spain and he is currently working on his Ph.D. degree in the UPV. From 2009 he is working in the Electronics and Communications Department of the ULA, teaching in the electrical and electronical area. From 2013 he has been with the Electronics Engineering Department, UPV, where he is with the Industrial Electronic Systems Group (GSEI), <http://gsei.upv.es>. His main research interests and fields are power converter modeling and control, integration and management of the distributed power sources in microgrids.

**Silvia Marzal** was born in Valencia, Spain, in 1984. He received the Ingeniero Telecomunicaciones (M.Sc) degree, in 2010 from the Universitat Politècnica de València (UPV), Spain and she is currently working on her Ph.D. degree studies on UPV, Spain. In 2012 he was with the Institute Center for Transportation and Territory on UPV, where she was involved in the design of communications systems applied to railway applications. From 2014, she has been with the Electronics Engineering Department, UPV, where she is with the Industrial Electronic Systems Group (GSEI), <http://gsei.upv.es>. Her main research interests and fields are communications protocols and topologies design and development, to control and manage the distributed power sources in microgrids.

**Raúl González-Medina** was born in Valencia, Spain, in 1978. He received the Ingeniero Industrial (M.Sc.) degree in 2005 and the Dr. en Ingeniería Electrónica Ph.D. degree in 2015, from the Universitat Politècnica de València (UPV). In 2005, he joined the Department of Electronics Engineering at the UPV, and got involved with the Industrial Electronic System Group (GSEI) where he is an R&D engineer, focused on technology transfer to companies. His main research interests

and fields are power converters, modulation techniques, grid-connected inverters, and converters for renewable energy sources. Since 2015, he is also teaching power electronics in the Department of Electronic Engineering at the UPV.

**Emilio Figueres** received the M.Sc. degree from the Ecole Nationale Supérieure d'Electrotechnique, d'Electronique, d'Informatique et d'Hydraulique de Toulouse, Toulouse, France, in 1995, and the Dr. Ingeniero Industrial (Ph.D.) degree from the Universitat Politècnica de València (UPV), Valencia, Spain, in 2001. Since 1996, he has been with the Electronics Engineering Department, UPV, where he is currently a Full Professor and the Head of the Department. He has coauthored more than 100 papers published in JCR indexed journals and conferences. He also holds 3 patents and was a co-recipient of the best paper award published in 2012 in the IEEE Transactions on Industrial Electronics. His main research interests include modeling and control of power converters, power processing of renewable energy sources, and grid connected converters for distributed power generation and improvement of power quality.

**Gabriel Garcerá** received the M.Sc. and Ph.D. degrees, both in Electrical Engineering, from the Universitat Politècnica de València (UPV) in 1993 and 1998, respectively. From 1993 to 1995 he was with the R&D Department of the company GH Group, involved in the design of switch-mode power supplies for particle accelerators at CERN. By the end of 1995 he joined the Electronics Engineering Department of the UPV, where he is currently a Full Professor. He is coauthor of more than 100 papers about power electronics in international journals and conferences. He has advised 13 Ph.D. Thesis. He was a co-recipient of the best paper award published in 2012 in the IEEE Transactions on Industrial Electronics (TIE). Since 2004, he is an Associate Editor of TIE. His main research interests and fields are in power converter modeling and control, power supplies, power converters for renewable energy sources, microgrids and electric vehicles battery chargers.